ACS APPLIED MATERIALS & INTERFACES

Research Article

www.acsami.org

Enhanced Performance of ZnO Piezotronic Pressure Sensor through Electron-Tunneling Modulation of MgO Nanolayer

Xinqin Liao,[†] Xiaoqin Yan,[†] Pei Lin,[†] Shengnan Lu,[†] Yuan Tian,[†] and Yue Zhang*[,†,‡]

[†]State Key Laboratory for Advanced Metals and Materials, School of Materials Science and Engineering, University of Science and Technology Beijing, Beijing 100083, People's Republic of China

[‡]Key Laboratory of New Energy Materials and Technologies, University of Science and Technology Beijing, Beijing 100083, People's Republic of China

ABSTRACT: Piezoelectric materials can be applied into electromechanical conversion and attract extensive attention with potential applications in various sensors. Here, we present two types of piezotronic pressure sensors based on ZnO nanoarrays. By introducing an insulating MgO (*i*-MgO) nanolayer, the "on/off" current ratio of the sensor is significantly improved up to 10^5. Furthermore, the sensor shows a high sensitivity of 7.1×10^4 gf^{-1}, a fast response time of 128 ms. The excellent properties are attributed to the combination of piezoelectric effect of ZnO nanoarrays and electron-tunneling modulation of MgO nanolayer, and the reversible potential barrier height controlled by piezoelectric potential. We further investigate the service behavior of the sensor, which can detect force varying from 3.2 to 27.2 gf. Our research provides a promising approach to boost the performance of nanodevices.

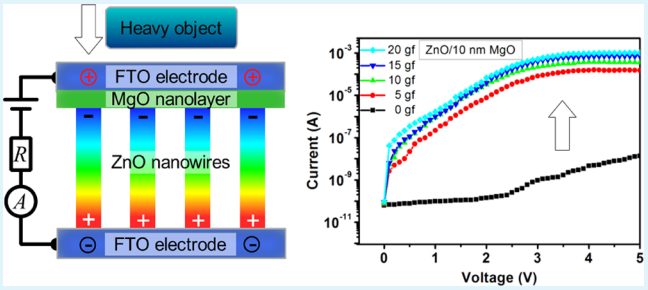

KEYWORDS: *piezoelectric effect, electron tunneling, ZnO nanoarrays, insulator−MgO nanolayer, pressure sensors*

INTRODUCTION

Structural health monitoring, which primarily consists of strain sensors (pressure sensors), is extremely significant to measure physical quantities of infrastructures, such as aircrafts, ships, automobiles, buildings, and railways.[1] To date, various nanomaterials, including nanoparticles,[2,3] nanowires,[4−12] nanofibers,[13−15] and nanotubes,[16−18] have been used for the achievement of novel sensors. These nanomaterials-based sensors are major based on force-induced changes in resistivity,[2,10,11,13,15−18] capacitance,[7,12] or piezoelectricity.[4−6,8,9,14] The advantage of piezoelectric pressure sensors lies at relatively low energy consumption in operation. It is of great significance for energy conservation.[9,19] Furthermore, piezoelectric effect combined with other effects can be utilized for enhancing performance of devices, such as photodetectors, humidity sensors.[20−22]

Zinc oxide (ZnO) is typical piezoelectric-material owing to noncentrosymmetric crystal structure.[5,6,8−10,23−29] This semiconductor material is harmless to environment[29−32] and gains widespread attention to pursued to design pressure sensors.[5,6,8−10,24] The recently developed ZnO pressure sensors based on a single nanowire have high sensitivity to load fluctuation, due to so small of sensing material that can response to tiny vibrancy.[5,8,9,24] In addition, the sensitivity of the devices can be further improved through the piezo-modulated interface engineering with appropriate structure designs. Via reversible Schottky-barrier height controlled by piezoelectric potential, the on/off current ratio can reach 120,[24] while the current value is small (10 μA, at 1 V with strain ~0.39%[6]). Research on single nanowire sensors provides a strong theoretical foundation for future extensive applications, such as multitudinous nanowire/nanorod arrays (NWAs/NRAs) prepared into devices. Recently, a large area of NWAs/NRAs was integrated into devices to obtain a large current value.[7,33] Nevertheless, the switch ratio (SR) is only ~100 at 3 V.[33] It is worth mentioning that a 10^4−10^7 scales SR of field-effect transistors or ultraviolet (UV) detectors is achieved by inserting insulating materials, due to the mechanism of electrons trap-assisted tunneling.[34−37] These insulating materials also promoted the characteristics of nanogenerators and spintronic devices.[38,39] However, to the best of our knowledge, relatively little work has been done to combine insulating dielectric property with piezo-modulated interface engineering in sensors.

Herein, we present pressure sensors based on ZnO NRAs. Typically, the SR achieved 10^5 by exploiting ultrathin magnesium oxide (MgO) insulating/barrier layer, which played a crucial role in modulating carrier transport and improving sensitivity of the sensors. The piezoelectric effect coupled with electron-tunneling modulation would be a promising means for performance optimization of other piezotronic devices.

Received: October 13, 2014
Accepted: January 6, 2015
Published: January 6, 2015

DOI: 10.1021/am5070443
ACS Appl. Mater. Interfaces 2015, 7, 1602−1607

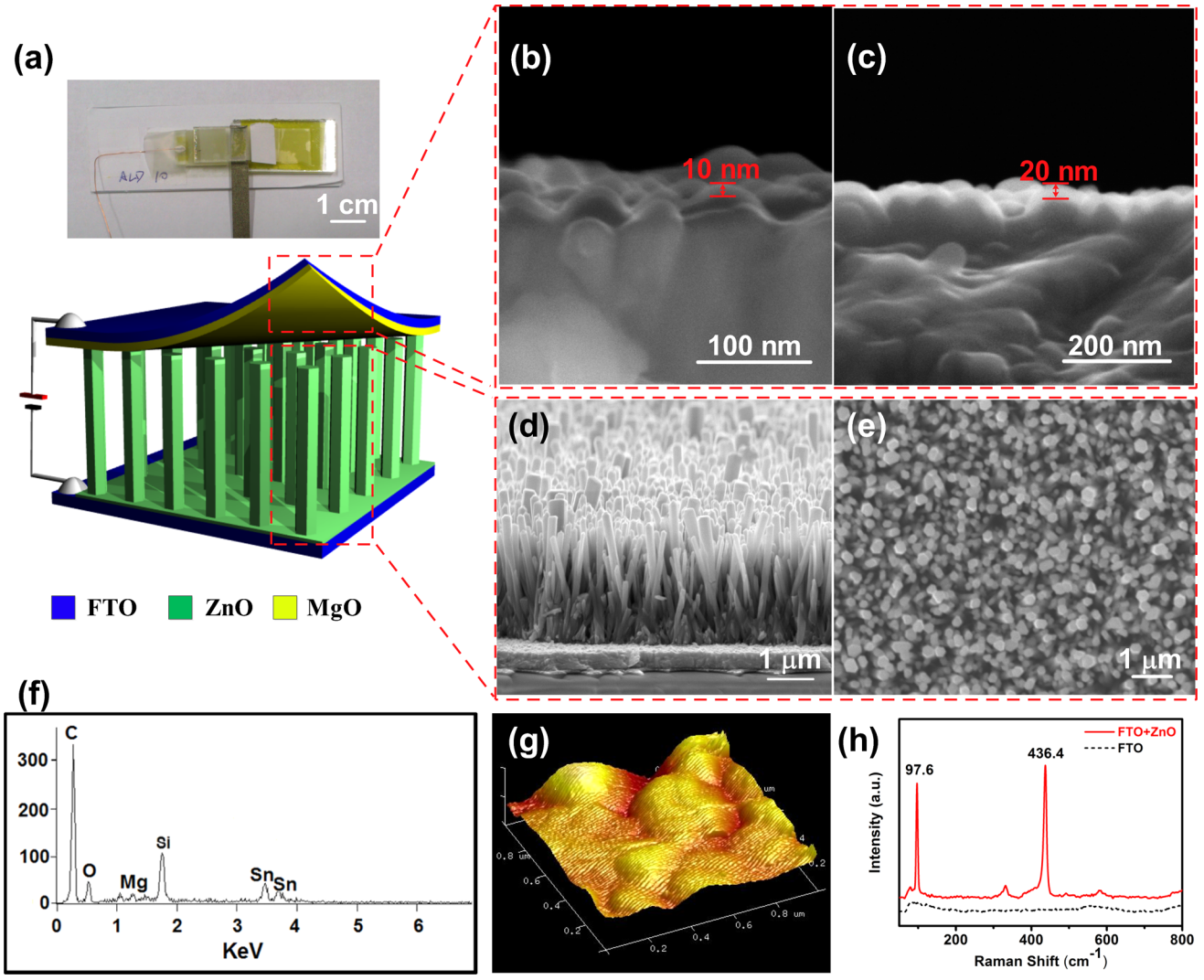

Figure 1. (a) The model of a pressure sensor. The field emission scanning electron microscopy (FESEM) images of (b) 10 and (c) 20 nm MgO layers deposited onto the FTO glass. (d and e) Cross-sectional and top-view FESEM images showing the morphologies of vertically aligned ZnO nanoarrays. (f and g) EDS and AFM images of the 10 nm MgO layer. (h) Raman spectra obtained from ZnO nanoarrays/FTO and pure FTO glass.

EXPERIMENTAL SECTION

The ZnO-NRAs were prepared by a hydrothermal method.[6,30,33] A ZnO seed layer was obtained by spin-coating a seed solution (0.5 M) of equal molar ethanolamine [C_2H_7NO] and zinc acetate dihydrate [$Zn(CH_3COO)_2{\cdot}2H_2O$] dissolved in ethylene glycol monomethyl ether (EGME) onto a fluorine-doped tin oxide (FTO) glass and then annealed at 623 K for half an hour. The precursor solution was an aqueous solution of hexamethylenetetramine (HMTA) and zinc nitrate hexahydrate [$Zn(NO_3)_2{\cdot}6H_2O$] with a concentration of 50 mM. The FTO glass coated with the seed crystal film was put into precursor solution, and the process was conducted at 368 K for 20 h. Subsequently, a part of the modified FTO glass was selectively etched with hydrochloric acid, where the electrode was led out. The next step was to deposit an ultrathin MgO film onto another FTO glass via the method of atomic layer deposition. Then, the two different FTO glasses were bonded together in the vertical direction. Finally, the contact was packaged well with polydimethylsiloxane (PDMS).

In all of the test procedures, the reference electrode was the FTO with the ZnO nanoarrays, and the potential was 0 V. Field emission scanning electron microscope (FESEM, SUPRA55) was employed to observe the morphology of synthesized materials. The Raman spectrum was obtained by utilizing confocal Raman spectroscopy (JY-HR800) with an Ar^+ laser source at room temperature. The surface morphology and elemental analysis were carried out using atomic force microscopy (AFM, Nanoscope IIIa, Multimode) and energy dispersive X-ray spectroscopy (EDS). The electromechanical properties of the pressure sensors were measured with semiconductor characterization system (Keithley 4200) under atmospheric pressure.

RESULTS AND DISCUSSION

Figure 1 illustrates the morphologies and characterization of components of the device with *i*-MgO. Figure 1a presents the optical photograph and schematic diagram of the sensor, which is composed of two different FTO glasses modified with MgO nanolayer and ZnO NRAs, respectively. In Figure 1b,c, two different thicknesses (10 and 20 nm) of MgO layers are identified. Figure 1f shows an energy dispersive spectroscopic (EDS) image of the 10 nm layer, which is deposited onto fluorine-doped tin oxide (FTO) glass. In Figure 1g, the continuous nanolayer is further confirmed by AFM. In addition, the mean diameter of orderly ZnO NRAs is 100 nm and the average length is 4 μm (Figure 1d,e). Figure 1h shows the Raman spectra of the ZnO nanoarrays/FTO and pure FTO glass, respectively. The peaks at 97.6 and 436.4 cm^{-1} are allocated to E_{2L} and E_{2H} modes of ZnO, which are the main characteristic peaks of Raman spectrum of ZnO. The intensities

DOI: 10.1021/am5070443
ACS Appl. Mater. Interfaces 2015, 7, 1602−1607

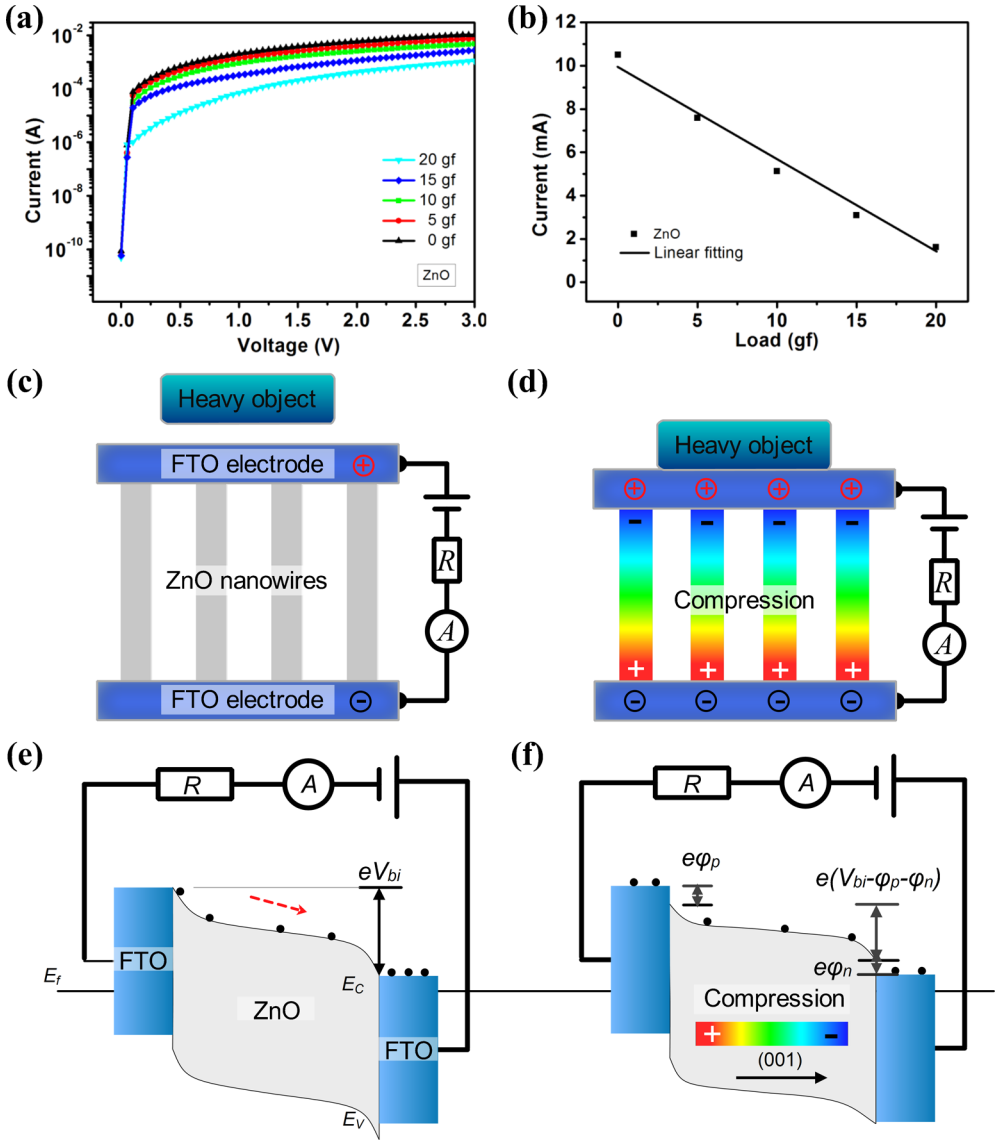

Figure 2. (a) The current–voltage (I–V) characteristic curves of the sensor with ZnO NRAs under different load conditions. (b) The relationship of current and force, obtained from graph a at 3 V. (c and d) Schematic diagram of working principle. The ribbons show the different piezoelectric potentials. (e and f) Band structure of the sensor under different loading conditions; black dots represent electrons, and red arrows represent the direction of electron movement.

of these two peaks indicate good crystal quality of ZnO because the intensity at 436.4 cm^{-1} is higher than the other peak.[40] In addition, the modes of multiphoton processes (E_{2L}–E_{2H}) and A_1 are observed at 331.7 and 589.6 cm^{-1}, respectively.

Typical current–voltage (I–V) characteristics of pressure sensor, which is based on ZnO NRAs, under various forces (1 gf = 0.0098 N), are shown in Figure 2a. The SR (I_f/I_0, I_f and I_0 are the final current under loading and unloading conditions, respectively) was 10.7 at 3 V. In addition, the sensitivity value S was -4.7×10^{-2} gf^{-1}, which was defined as $S = [\Delta I_f/I_0]/\Delta F$ (F is the applied force),[23] as depicted in Figure 2b.

The working principle and band structure of the sensor only based on ZnO NRAs are demonstrated in Figure 2c–f. First, we know the power of electrons movement is energy difference. Lower the energy difference, the electrons move slowly. As the piezoelectric potential was modulated by a stress applied at c axis of ZnO,[25−27] the negative pressure electric potential φ_n is generated at the top surface of ZnO, and then the energy band of ZnO ascends. On the other aspect, the positive potential φ_p at the bottom surface of ZnO pulls down the energy band. Accordingly, the energy difference, between top and bottom surface of ZnO, is reduced from eV_{bi} to $e(V_{bi} - \varphi_n - \varphi_p)$ (e is electron energy, and V_{bi} is the fixed bias voltage). Then, the results lead to the measured current decreased as the load increased. Furthermore, the magnitude of electric field through ZnO is calculated by the modified equation:[23]

$$\Delta E = V_{bi}/L - E_p = V_{bi}/L - \varepsilon/d \quad (1)$$

where L represents the length of ZnO NRAs, E_p is the piezoelectric field, ε is the strain of each nanowire, and d is the piezoelectric coefficient. Because the built-in potential is opposite to the external voltage and the potential gradually enlarges by the increase of the applied force, the magnitude of electric field is weakened. Then, the movement of electrons inside the ZnO reduces, which is driven by the electric field. Subsequently, the current monotonically decreases as the load increased at a fixed bias voltage (Figure 2b).

DOI: 10.1021/am5070443
ACS Appl. Mater. Interfaces 2015, 7, 1602–1607

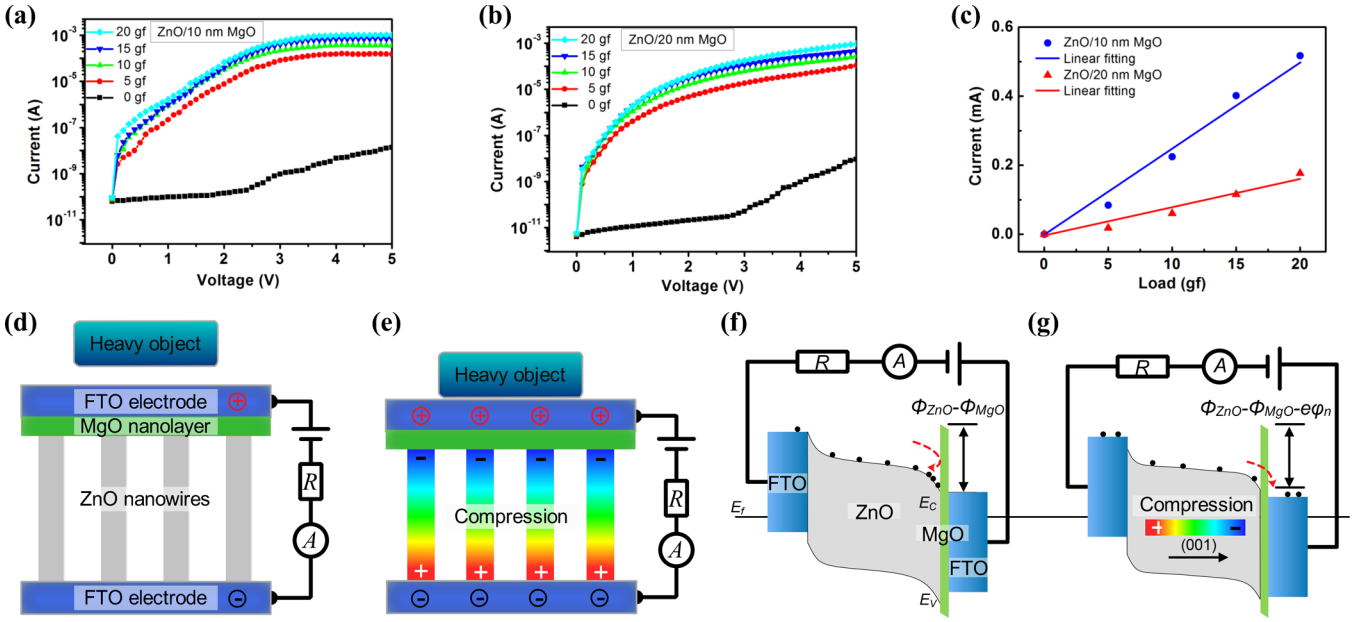

Figure 3. *I*–*V* characteristics of the sensors with (a) 10 or (b) 20 nm MgO layer. (c) Current versus force, obtained from graphs a and b at 3 V. (d and e) Schematic diagram of working principle. The ribbons show different piezoelectric potentials. (f and g) Band structure of the sensor under different loading conditions; black dots represent electrons, and red arrows represent electron movement.

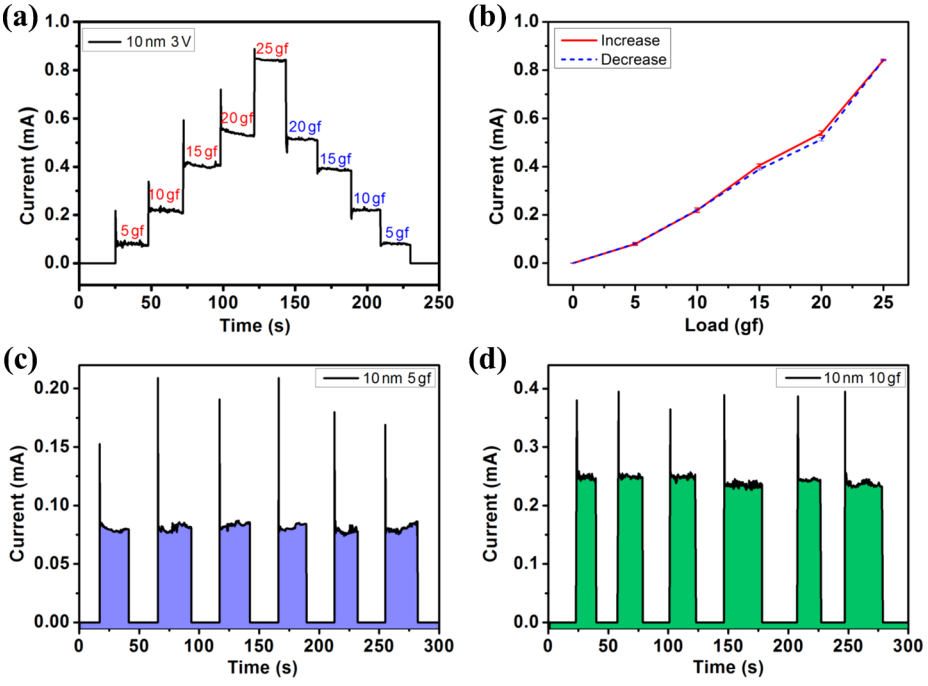

Figure 4. Current–time (*I*–*T*) curves of the sensor with 10 nm *i*-MgO under various forces at a fixed bias voltage of 3 V. (a) Two characteristic relationships between current and applied force. One is the current increasing with applied force, which adds from 0 to 25 gf at 5 gf each step, and the other is the current following with applied force decreased. (b) Current versus load; curves represent current responding with (red) increasing and (blue) decreasing loads. Current response under circular loading at (c) 5 and (d) 10 gf.

We also achieved another two pressure sensors with 10 or 20 nm *i*-MgO nanolayer. In Figure 3a,b, the current values of the sensors fluctuated at 10^{-11} to 10^{-8} A scales between 0 to +5 V under 0 gf. Compared with Figure 2a, we found that the values were very small. The SRs were yet 7.2×10^5 and 5.4×10^5, respectively, which were considerably larger than the ratio of sensor without *i*-MgO. Moreover, the sensitivity values reached to 7.1×10^4, 1.9×10^4 gf^{-1}, respectively (Figure 3c).

The working principle and band structure of the sensor with *i*-MgO are presented in Figure 3d–g. As recognized, Φ_{ZnO} (the electron affinity of ZnO) is 4.35–4.5 eV and Φ_{MgO} is 0.85 eV.[41−43] There is a potential barrier ($\Delta\Phi = \Phi_{ZnO} - \Phi_{MgO}$) at ZnO/MgO interface. When a heavy object is far away from the sensor, most electrons cannot flow into the barrier layer due to insufficient energy for electronic transition. While ZnO NRAs are compressed by the pressure, the negative pressure electric potential is generated at the top surface of ZnO beside the

DOI: 10.1021/am5070443
ACS Appl. Mater. Interfaces 2015, 7, 1602–1607

ZnO/MgO interface and can be further raised by the increase of the applied force. Then, the energy band of ZnO ascends, which is modulated by electric potential. Subsequently, the barrier height is relatively lowered for the electrons inside ZnO. Equivalently, more electrons have enough energy to surmount the potential barrier. Notably, piezoelectric effects also slow the movement of electrons at this moment, but enough activated electrons still tunnel through and bother the barrier layer. In the case of relatively low barrier height modulated by piezoelectric potential, the activated electrons will surmount the barrier layer. Thus, the current of the sensor with *i*-MgO is increased as the load increased, is controlled by the applied pressure, and has linear relationship with the force (Figure 3c). In addition, as the 20 nm layer is too thick to allow more electrons to easily tunnel through the barrier layer, the performance of the sensor with 10 nm *i*-MgO is slightly better.

The physical robustness and reliability of the pressure sensor with 10 nm *i*-MgO were evaluated by subjecting them to a series of force cycles under dynamic loading condition, when a fixed bias voltage of 3 V was applied. The electromechanical properties of the sensor were measured by monitoring the current under different force level. We can control the force to modulate the potential barrier height and then to change the current value. As it was applied with a force, the current was fixed at a certain value (Figure 4a). Figure 4b depicted the hysteresis curve related between the current and the force. Notably, there was almost a one-to-one correspondence between the force and the current value and negligible hysteresis in the response of the pressure sensor. Furthermore, the sensor responded rapidly at every turning point within 128 ms, and the current remained identical under the same force cycles (5 or 10 gf, Figure 4c,d).

We further investigated the service behavior of the sensor with 10 nm *i*-MgO. As shown in Figure 5, when the load was

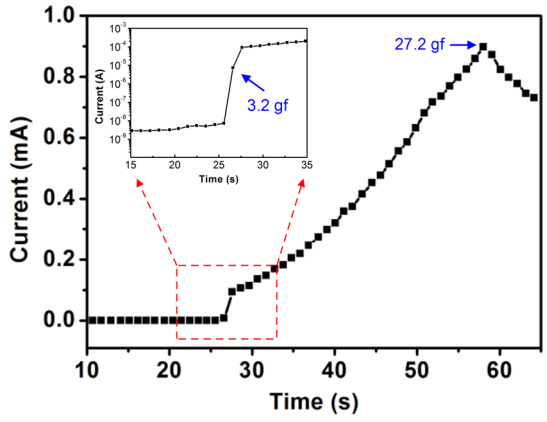

Figure 5. Current response of the pressure sensor with 10 nm *i*-MgO under continuous loading at 1.0 gf/s when operated at a fixed bias voltage of 3 V. Inset is an enlarged view of a part.

less than 3.2 gf, the sensor was invalid to detect the force. Subsequently, the current increased almost linearly with the applied force up to 27.2 gf and then began to decrease. This phenomenon is the result of interaction of the controllable potential barrier at ZnO/MgO interface and the electric field inside ZnO NRAs and can be divided into three stages. At the stage of a small force applied, the enormous electrons are activated by the electric field. However, the potential barrier is too high for the most activated electrons to tunnel through the MgO nanolayer. When the potential barrier falls below a certain threshold through the energy band raised by the pressure electric potential generated by the applied force increasing, more activated electrons surmount the barrier layer at the second stage, although the activated electrons has decreased gradually due to the electric field weakened by the pressure electric potential generated by the applied force. At the last stage, though the potential barrier height decreases continuously, fewer and fewer electrons are activated leading to the current decrease.

CONCLUSION

In summary, we have successfully constructed two types of piezotronic pressure sensor. We found the MgO nanolayer, which acted as a carrier control layer, could significantly improve the performance of the devices, and the effect of 10 nm layer was superior to that of the 20 nm layer effect. The piezoelectric sensor based only on ZnO NRAs showed a small SR of 10.7, a sensitivity of -4.7×10^{-2} gf^{-1} at 3 V. The pressure sensor with 10 nm *i*-MgO demonstrated excellent performance and featured a small "off" current, an ultrahigh SR (7.2×10^5), which was higher than the ratio (5.4×10^5) of the sensor with 20 nm *i*-MgO. In addition, it showed characteristics of fast response (128 ms), a high sensitivity (7.1×10^4 gf^{-1}), good stability under different loading condition, and an approximately linear relationship between current and applied force in the range of 3.2−27.2 gf at a fixed voltage of 3 V. The innovation of piezoelectric effect combined with electron-tunneling modulation may provide an alternative route to improve the performance of other nanosensors.

AUTHOR INFORMATION

Corresponding Author

*E-mail: yuezhang@ustb.edu.cn. Tel.: +86-010-62334725.

Notes

The authors declare no competing financial interest.

ACKNOWLEDGMENTS

This work was supported by the National Major Research Program of China (2013CB932602), the Major Project of International Cooperation and Exchanges (2012DFA50990), the Program of Introducing Talents of Discipline to Universities, NSFC (51232001, 51172022, 51372023, 51372020), the Research Fund of Co-construction Program from Beijing Municipal Commission of Education, the Fundamental Research Funds for the Central Universities, and the Program for Changjiang Scholars and Innovative Research Team in University.

REFERENCES

(1) Farrar, C. R.; Worden, K. An Introduction to Structural Health Monitoring. *Philos. Trans. R. Soc., A* **2007**, *365*, 303−315.

(2) Farcau, C.; Sangeetha, N. M.; Moreira, H.; Viallet, B.; Grisolia, J.; Pradines, D. C.; Ressier, L. High-Sensitivity Strain Gauge based on a Single Wire of Gold Nanoparticles Fabricated by Stop-and-Go Convective Self-Assembly. *ACS Nano* **2011**, *5*, 7137−7143.

(3) Sreeprasad, T. S.; Rodriguez, A. A.; Colston, J.; Graham, A.; Shishkin, E.; Pallem, V.; Berry, V. Electron-Tunneling Modulation in Percolating Network of Graphene Quantum Dots: Fabrication, Phenomenological Understanding, and Humidity/Pressure Sensing Applications. *Nano Lett.* **2013**, *13*, 1757−1763.

(4) Hu, Y.; Chang, Y.; Fei, P.; Snyder, R. L.; Wang, Z. L. Designing the Electric Transport Characteristics of ZnO Micro/Nanowire

DOI: 10.1021/am5070443
ACS Appl. Mater. Interfaces 2015, 7, 1602−1607

Devices by Coupling Piezoelectric and Photoexcitation Effects. *ACS Nano* **2010**, *4*, 1234−1240.
(5) Xiao, X.; Yuan, L.; Zhong, J.; Ding, T.; Liu, Y.; Cai, Z.; Rong, Y.; Han, H.; Zhou, J.; Wang, Z. L. High-Strain Sensors Based on ZnO Nanowire/Polystyrene Hybridized Flexible Films. *Adv. Mater.* **2011**, *23*, 5440−5444.
(6) Han, W.; Zhou, Y.; Zhang, Y.; Chen, C.; Lin, L.; Wang, X.; Wang, S.; Wang, Z. L. Strain-Gated Piezotronic Transistors Based on Vertical Zinc Oxide Nanowires. *ACS Nano* **2012**, *6*, 3760−3766.
(7) Hu, W.; Niu, X.; Zhao, R.; Pei, Q. Elastomeric Transparent Capacitive Sensors based on an Interpenetrating Composite of Silver Nanowires and Polyurethane. *Appl. Phys. Lett.* **2013**, *102*, 083303.
(8) Lu, S.; Qi, J.; Wang, Z.; Lin, P.; Liu, S.; Zhang, Y. Size Effect in a Cantilevered ZnO Micro/Nanowire and Its Potential as a Performance Tunable Force Sensor. *RSC Adv.* **2013**, *3*, 19375−19379.
(9) Liao, Q.; Mohr, M.; Zhang, X.; Zhang, Z.; Zhang, Y.; Fecht, H. J. Carbon Fiber-ZnO Nanowire Hybrid Structures for Flexible and Adaptable Strain Sensors. *Nanoscale* **2013**, *5*, 12350−12355.
(10) Amjadi, M.; Pichitpajongkit, A.; Lee, S.; Ryu, S.; Park, I. Highly Stretchable and Sensitive Strain Sensor Based on Silver Nanowire-Elastomer Nanocomposite. *ACS Nano* **2014**, *8*, 5154−5163.
(11) Gong, S.; Schwalb, W.; Wang, Y.; Chen, Y.; Tang, Y.; Si, J.; Shirinzadeh, B.; Cheng, W. A Wearable and Highly Sensitive Pressure Sensor with Ultrathin Gold Nanowires. *Nat. Commun.* **2014**, *5*, 3132.
(12) Yao, S.; Zhu, Y. Wearable Multifunctional Sensors Using Printed Stretchable Conductors Made of Silver Nanowires. *Nanoscale* **2014**, *6*, 2345−2352.
(13) Pang, C.; Lee, G. Y.; Kim, T.; Kim, S. M.; Kim, H. N.; Ahn, S.; Suh, K. A Flexible and Highly Sensitive Strain-Gauge Sensor Using Reversible Interlocking of Nanofibres. *Nat. Mater.* **2012**, *11*, 795−801.
(14) Persano, L.; Dagdeviren, C.; Su, Y.; Zhang, Y.; Girardo, S.; Pisignano, D.; Huang, Y.; Rogers, J. High Performance Piezoelectric Devices Based on Aligned Arrays of Nanofibers of Poly(vinylidenefluoride-co-trifluoroethylene). *Nat. Commun.* **2013**, *4*, 1633.
(15) Yan, C.; Wang, J.; Kang, W.; Cui, M.; Wang, X.; Foo, C. Y.; Chee, K. J.; Lee, P. S. Highly Stretchable Piezoresistive Graphene-Nanocellulose Nanopaper for Strain Sensors. *Adv. Mater.* **2014**, *26*, 2022−2027.
(16) Yamada, T.; Hayamizu, Y.; Yamamoto, Y.; Yoshiki, Y.; Najafabadi, A. I.; Futaba, D. N.; Hata, K. A Stretchable Carbon Nanotube Strain Sensor for Human-Motion Detection. *Nat. Nanotechnol.* **2011**, *6*, 296−301.
(17) Takei, K.; Yu, Z.; Zheng, M.; Ota, H.; Takahashi, T.; Javey, A. Highly Sensitive Electronic Whiskers based on Patterned Carbon Nanotube and Silver Nanoparticle Composite Films. *Proc. Natl. Acad. Sci. U.S.A.* **2014**, *111*, 1703−1707.
(18) Kim, B.; Jang, S.; Geier, M.; Prabhumirashi, P. L.; Hersam, M. C.; Dodabalapur, A. High Speed, Inkjet Printed Carbon Nanotube/Zinc Tin Oxide Hybrid Complementary Ring Oscillators. *Nano Lett.* **2014**, *14*, 3683−3687.
(19) Liao, Q.; Zhang, Z.; Zhang, X.; Mohr, M.; Zhang, Y. Flexible Piezoelectric Nanogenerators Based on a Fiber/ZnO Nanowires/Paper Hybrid Structure for Energy Harvesting. *Nano Res.* **2014**, *7*, 917−928.
(20) Yu, R.; Pan, C.; Hu, Y.; Li, L.; Liu, H.; Liu, W.; Chua, S.; Chi, D.; Wang, Z. L. Enhanced Performance of GaN Nanobelt-Based Photodetectors by Means of Piezotronic Effects. *Nano Res.* **2013**, *6*, 758−766.
(21) Lin, P.; Chen, X.; Yan, X.; Zhang, Z.; Yuan, H.; Li, P.; Zhao, Y.; Zhang, Y. Enhanced Photoresponse of Cu_2O/ZnO Heterojunction with Piezo-Modulated Interface Engineering. *Nano Res.* **2014**, *7*, 860−868.
(22) Hu, G.; Zhou, R.; Yu, R.; Dong, L.; Pan, C.; Wang, Z. L. Piezotronic Effect Enhanced Schottky-Contact ZnO Micro/Nanowire Humidity Sensors. *Nano Res.* **2014**, *7*, 1083−1091.
(23) Wang, Z. L.; Song, J. Piezoelectric Nanogenerators Based on Zinc Oxide Nanowire Arrays. *Science* **2006**, *312*, 242−246.
(24) Zhou, J.; Fei, P.; Gu, Y.; Mai, W.; Gao, Y.; Yang, R.; Bao, G.; Wang, Z. L. Piezoelectric-Potential-Controlled Polarity-Reversible Schottky Diodes and Switches of ZnO Wires. *Nano Lett.* **2008**, *8*, 3973−3977.
(25) Wang, Z. L. Piezotronic and Piezophototronic Effects. *J. Phys. Chem. Lett.* **2010**, *1*, 1388−1393.
(26) Zhang, Y.; Yan, X. Q.; Yang, Y.; Huang, Y.; Liao, Q.; Qi, J. Scanning Probe Study on the Piezotronic Effect in ZnO Nanomaterials and Nanodevices. *Adv. Mater.* **2012**, *24*, 4647−4655.
(27) Yang, Y.; Guo, W.; Wang, X.; Wang, Z.; Qi, J.; Zhang, Y. Size Dependence of Dielectric Constant in a Single Pencil-Like ZnO Nanowire. *Nano Lett.* **2012**, *12*, 1919−1922.
(28) Lin, P.; Yan, X.; Zhang, Z.; Shen, Y.; Zhao, Y.; Bai, Z.; Zhang, Y. Self-Powered UV Photosensor Based on PEDOT:PSS/ZnO Micro/Nanowire with Strain-Modulated Photoresponse. *ACS Appl. Mater. Interfaces* **2013**, *5*, 3671−3676.
(29) Li, P.; Liao, Q.; Yang, S.; Bai, X.; Huang, Y.; Yan, X.; Zhang, Z.; Liu, S.; Lin, P.; Kang, Z.; Zhang, Y. In Situ TEM Investigation on Fatigue Behavior of Single ZnO Wires under High-Cycle Strain. *Nano Lett.* **2014**, *14*, 480−485.
(30) Zhang, X. M.; Lu, M. Y.; Zhang, Y.; Chen, L.; Wang, Z. L. Fabrication of a High-Brightness Blue-Light-Emitting Diode Using a ZnO-Nanowire Array Grown on p-GaN Thin Film. *Adv. Mater.* **2009**, *21*, 2767−2770.
(31) Zhang, Y.; Yang, Y.; Wang, Z. L. Piezo-Phototronics Effect on Nano/Microwire Solar Cells. *Energy Environ. Sci.* **2012**, *5*, 6850−6856.
(32) Lei, Y.; Luo, N.; Yan, X.; Zhao, Y.; Zhang, G.; Zhang, Y. A Highly Sensitive Electrochemical Biosensor based on Zinc Oxide Nanotetrapods for L-Lactic Acid Detection. *Nanoscale* **2012**, *4*, 3438−3443.
(33) Zhang, Z.; Liao, Q.; Yan, X.; Wang, Z. L.; Wang, W.; Sun, X.; Lin, P.; Huang, Y.; Zhang, Y. Functional Nanogenerators as Vibration Sensors Enhanced by Piezotronic Effects. *Nano Res.* **2014**, *7*, 1−9.
(34) Du, X.; Mei, Z.; Liu, Z.; Guo, Y.; Zhang, T.; Hou, Y.; Zhang, Z.; Xue, Q.; Kuznetsov, A. Y. Controlled Growth of High-Quality ZnO-Based Films and Fabrication of Visible-Blind and Solar-Blind Ultra-Violet Detectors. *Adv. Mater.* **2009**, *21*, 4625−4630.
(35) Ganjipour, B.; Wallentin, J.; Borgström, M. T.; Samuelson, L.; Thelander, C. Tunnel Field-Effect Transistors Based on InP−GaAs Heterostructure Nanowires. *ACS Nano* **2012**, *6*, 3109−3113.
(36) Le, S. T.; Jannaty, P.; Luo, X.; Zaslavsky, A.; Perea, D. E.; Dayeh, S. A.; Picraux, S. T. Axial SiGe Heteronanowire Tunneling Field-Effect Transistors. *Nano Lett.* **2012**, *12*, 5850−5855.
(37) Sreeprasad, T. S.; Rodriguez, A. A.; Colston, J.; Graham, A.; Shishkin, E.; Pallem, V.; Berry, V. Electron-Tunneling Modulation in Percolating Network of Graphene Quantum Dots: Fabrication, Phenomenological Understanding, and Humidity/Pressure Sensing Applications. *Nano Lett.* **2013**, *13*, 1757−1763.
(38) Hinchet, R.; Lee, S.; Ardila, G.; Montes, L.; Mouis, M.; Wang, Z. L. Performance Optimization of Vertical Nanowire-based Piezoelectric Nanogenerators. *Adv. Funct. Mater.* **2014**, *24*, 971−977.
(39) Miwa, S.; Ishibashi, S.; Tomita, H.; Nozaki, T.; Tamura, E.; Ando, K.; Mizuochi, N.; Saruya, T.; Kubota, H.; Yakushiji, K.; Taniguchi, T.; Imamura, H.; Fukushima, A.; Yuasa, S.; Suzuki, Y. Highly Sensitive Nanoscale Spin-Torque Diode. *Nat. Mater.* **2014**, *13*, 50−56.
(40) Damen, T. C.; Porto, S. P. S.; Tell, B. Raman Effect in Zinc Oxide. *Phys. Rev.* **1966**, *142*, 570−574.
(41) Heiland, G.; Mollwo, E.; Stöckmann, F. Electronic Processes in Zinc Oxide. *Solid State Phys.* **1959**, *8*, 191−323.
(42) Lu, M. Y.; Song, J.; Lu, M. P.; Lee, C. Y.; Chen, L. J.; Wang, Z. L. ZnO−ZnS Heterojunction and ZnS Nanowire Arrays for Electricity Generation. *ACS Nano* **2009**, *3*, 357−362.
(43) Roessler, D. M.; Walker, W. C. Electronic Spectrum and Ultraviolet Optical Properties of Crystalline MgO. *Phys. Rev.* **1967**, *159*, 733−738.

DOI: 10.1021/am5070443
ACS Appl. Mater. Interfaces 2015, 7, 1602−1607